

Article

Earthquake Response Modeling of Corroded Reinforced Concrete Hollow-Section Piers via Simplified Fiber-Based FE Analysis

Nicola Scattarreggia ¹, Tianyue Qiao ² and Daniele Malomo ^{2,*}¹ University School for Advanced Studies (IUSS), 27100 Pavia, Italy; nicola.scattarreggia@iusspavia.it² Department of Civil Engineering, McGill University, Montréal, QC H3A 0C3, Canada; tianyue.qiao@mail.mcgill.ca

* Correspondence: daniele.malomo@mcgill.ca

Abstract: The effect of corrosion-induced damage on the seismic response of reinforced concrete (RC) circular bridge piers has been extensively investigated in the last decade, both experimentally and numerically. Contrarily, only limited research is presently available on hollow-section members, largely employed worldwide and intrinsically more vulnerable to corrosion attacks. In this paper, fiber-based finite element (FB-FEM) models, typically the preferred choice by practitioners given their reduced computational expense, are validated against previous shake-table and quasi-static cyclic tests on hollow-section RC columns, and then used to investigate the influence of corrosion-induced damage. To this end, modeling strategies of varying complexity are used, including artificial reduction of steel rebar diameter, yield strength and ductility, as well as that of concrete compressive strength to simulate cover loss, and ensuing dissimilarities quantified. Pushover and incremental dynamic analyses are conducted to explore impacts on collapse behavior, extending experimental results while accounting for multiple corrosion rates. Produced outcomes indicate a minimal influence of cover loss; substantial reductions of base shear (up to 37%) and ultimate displacement capacity (up to 50%) were observed, instead, when introducing relevant levels of deterioration due to corrosion (i.e., 30% rebar mass loss). Its predicted impact is generally lower when considering more simplified assumptions, which may thus yield non-conservative predictions.

Keywords: corrosion; modeling; bridges; hollow-section; fiber-based; finite element method

Citation: Scattarreggia, N.; Qiao, T.; Malomo, D. Earthquake Response Modeling of Corroded Reinforced Concrete Hollow-Section Piers via Simplified Fiber-Based FE Analysis. *Sustainability* **2021**, *13*, 9342. <https://doi.org/10.3390/su13169342>

Academic Editors: Ime Bassey Obot, Amrbrish Singh, Akram Alfantazi and Ihsan Ulhaq Toor

Received: 23 July 2021

Accepted: 17 August 2021

Published: 20 August 2021

Publisher's Note: MDPI stays neutral with regard to jurisdictional claims in published maps and institutional affiliations.



Copyright: © 2021 by the authors. Licensee MDPI, Basel, Switzerland. This article is an open access article distributed under the terms and conditions of the Creative Commons Attribution (CC BY) license (<https://creativecommons.org/licenses/by/4.0/>).

1. Introduction

Corrosion of steel rebars in reinforced concrete (RC) bridges represents a major public safety threat for many communities all over the world, especially those in seismically-prone countries, whose infrastructures have often been built prior to the introduction of modern code provisions, are lacking proper maintenance, and exposed to climate change hazards [1]. In the United States, the estimated annual direct cost associated with bridge corrosion is around \$8.3 billion according to the U.S. Federal Highway Administration (FHWA) [2]. Analogous numbers characterize the infrastructure system of e.g., Canada, where it is expected that extreme climate conditions, such as cyclic precipitations and temperature fluctuations will increase over the next years [3], possibly worsening the already not ideal health conditions of existing RC bridges. In Europe, as in most other developed regions, the age profile of RC bridges typically reflects a peak in construction activities around 1960–1980, meaning that most of them have an age of 40 or more years, and they were designed for a service life of 50 years [4]. Corrosion-induced damage is further reducing their lifespan at an alarming pace, as well as those of similar bridges in other areas, already compromised by other concurrent factors as demonstrated by the recent series of disastrous collapses that occurred in, as examples, Asia [5] and South America [6].

At the member scale and from a bridge engineering perspective, as noted by [7], corrosion processes will make RC piers experience (i) a reduction of the mechanically-

effective section of reinforcement bars and (ii) volume expansion that generates splitting stresses in the concrete, which may crack and spall the concrete cover and affect the bond between the reinforcement and the concrete. As a result, when corroded RC members are subjected to earthquake actions, they typically exhibit a more brittle mechanical response with reduced ultimate displacement and peak force capacities, thus further increasing their seismic vulnerability. To assess the effect of the latter phenomena on seismic response, various experimental tests have been conducted, comparing the performance of standard and corroded loadbearing vertical elements [8–10]. However, carrying out full-scale and field tests on bridge components is challenging due to both costs and safety concerns issues [11,12]. Within this context, therefore, such investigations may benefit significantly from the use of reliable numerical methods able to represent the effects of corrosion-induced damage on mechanical behavior. To this end, a wide range of analytical [13], micro [14], meso [15] and macro-scale [16] models have been proposed and successfully applied so far. Among the simplified approaches typically preferred by practitioners and applied researchers, fiber-based finite element models (FB-FEM) are one of the most employed because of the acceptable compromise between accuracy and computational time.

In this framework, corrosion is typically represented through artificial diameter reduction of steel rebars, determined as a function of empirically-determined corrosion rates [17], while the experimentally-observed influence of concrete cover loss [18], reduced displacement capacity [19] and yield strength [20] of rebars is seldom accounted for numerically. To date, however, potential differences in terms of predicted outcomes produced by these different FB-FEM modeling approaches have not been compared yet, leaving engineering professionals without clear guidance. Recent applications span from the seismic assessment of existing RC buildings [21] to entire RC bridges [22] with both intact and corroded elements. Studies on circular RC columns have also been conducted using FB-FEM models [23,24], albeit none of them focus on hollow-section members, largely used for erecting RC bridges in many earthquake-prone countries because of their reduced cost and ease of construction with respect to more traditional solutions. Dedicated experimental tests have only recently become available [25], and thus presently are mainly comprised of characterization studies on small-scale samples.

Given the research gaps identified above, the aim of this work is two-fold. First, the seismic response of RC circular hollow-section bridge piers under various levels of corrosion-induced damage is investigated numerically using FB-FEM models, validated on previous tests on intact specimens [26]. Second, the modeling strategies mentioned above are scrutinized and ensuing results compared, to provide readers with an overview of potential differences and similarities in terms of simulated energy dissipation and force-displacement response under both quasi-static (monotonic, cyclic) and dynamic loading (experimentally-employed shake-table signal, incremental dynamic analysis—IDA).

2. Fiber Modeling Approach for RC Circular Hollow-Section Bridge Piers

In fiber modeling, the stress–strain state of RC representative sections is inferred integrating the nonlinear uniaxial response of the individual fibers in which the whole section is subdivided, distinguishing between those of steel, confined, and unconfined concrete. In the FB-FEM framework, structural members are idealized as frame elements with finite length and assigned cross-sections at selected integration points. In what follows, reference is made to the specific case of the modeling of RC hollow-section bridge piers. Interested readers may refer to, e.g., [22] for more detailed information on FB-FEM approaches, formulation and application to the seismic analysis of RC elements.

In Figure 1, a photo of the tested circular RC pier taken as a reference in this work is shown, along with its main dimensions and characteristics, as well as the corresponding FB-FEM numerical idealization. The specimen, tested at the Eucentre laboratory (Pavia, Italy) in 2008, as further discussed by Petrini et al. [26] who conducted the experiment, consisted of a reduced-scale (scaling factor of 4) RC hollow-section pier representative

of that typically is found in cantilever bridges, with a cross-section of 0.0975 m^2 and a gross-section moment of inertia of $I = 0.0017 \text{ m}^4$. Reinforcements are detailed in Figure 1a.

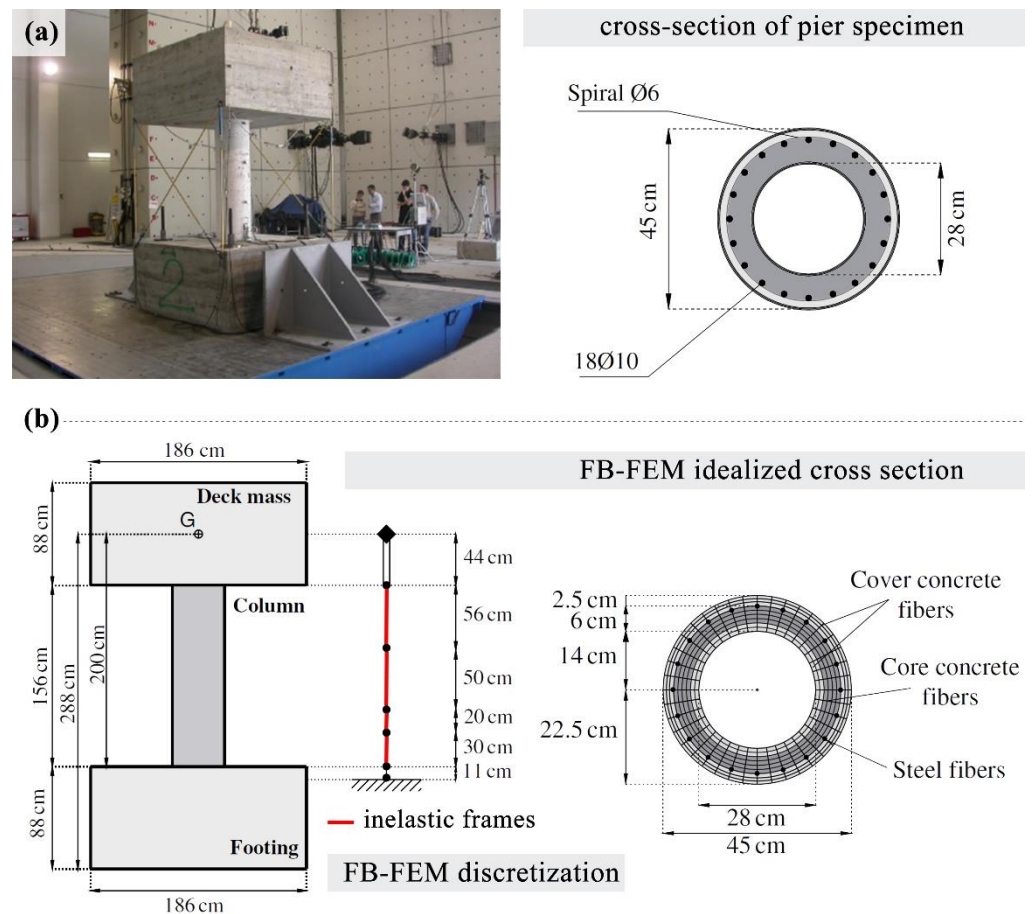


Figure 1. (a) Photo of experimental setup and cross section of the pier specimen, (b) FB-FEM idealization and numerical fiber modeling of pier cross-section (adapted from Petrini et al. [26]).

As stated in [26], the length of the plastic region at the pier bottom was assumed to be 45 cm, i.e., equal to the pier diameter, where a spiral $\phi 6@30$ mm with a transversal reinforcement ratio of $\rho_s = 0.93\%$ was used. In the remaining parts, a spiral $\phi 6@60$ mm was provided. To account for the vertical weight of the bridge deck and footing, a $1.86 \times 1.86 \times 0.88$ m top mass (RC block, 7.8 tons) was added and reinforced with 12 stirrups $\phi 12@1$ m; longitudinal bars of the column were fully anchored inside the two masses. The footing was anchored to the strong floor (cyclic test) or shake-table (dynamic test) with four post-tensioned vertical bars to avoid any relative displacement. Two main types of tests were conducted: quasi-static cyclic and dynamic shake-table. A cyclic loading protocol with eight main consecutive phases of varying target displacement was used for the quasi-static test, starting with 3 cycles up to 0.00085 m and then 0.0017 m, 0.013 m, 0.034 m, 1 cycle up to 0.017 m, 3 cycles up to 0.068 m, 1 cycle up to 0.017 m, and finally 3 cycles up to 0.1 m. For the shake-table, a Morgan Hill earthquake-like signal (1984, Halls Valley, Northern California, USA, $M_w = 6.2$, $PGA = 0.15$ g, where M_w is moment magnitude and PGA is peak ground acceleration) was amplified up to a $PGA = 1.2$ g.

To simulate both the experimental tests, the modeling strategy described below, implemented in the commercial software SeismoStruct [27] and graphically represented in Figure 1b, was adopted. The pier has been idealized with six frame elements, totaling a height of 2 m from the base up to the top mass center of gravity. As suggested by [22], whose work guided the development of the FB-FEM model presented herein, four main plastic regions were identified (highlighted in red color in Figure 1b) based on expected inelastic

response. The remaining parts of the column were defined as rigid. As shown in Figure 1b, 300 concentric fibers were modeled for representing longitudinal reinforcing bars, concrete cover, and confined regions, to which Menegotto and Pinto [28], Mander et al. [29], and Martinez-Rueda and Elnashai [30] models were assigned. Employed material parameters are summarized in Table 1 below, where f_c is compressive strength of concrete at 28 days, ε_c is compressive strain of unconfined concrete at maximum strength, f_t is tensile strength, k_1 , k_2 and k_3 are confinement (strength enhancement) factors allotted to core concrete confined by ϕ 6@30, core concrete confined by ϕ 6@60 and unconfined concrete cover. As per the steel properties, f_y is yield strength, E is Young's modulus, A_0 , A_1 , A_2 are model parameters controlling the transition from elastic to plastic branches, respectively, and, finally, A_3 and A_4 stand for isotropic hardening parameters.

Table 1. Material parameters implemented in the FB-FEM model.

f_c	ε_c	f_t	k_1	k_2	k_3	f_y	E	A_0	A_1	A_2	A_3	A_4
MPa	-	kPa	-	-	-	MPa	GPa	-	-	-	-	-
39	0.0025	0.001	1.35	1.18	1	514	210	20	18.5	0.15	0	0

3. Preliminary Validation Process against Test Results on Intact Specimens

In this section, experimental outcomes and numerical counterparts are compared to validate baseline models that will be used for corrosion impact analysis. As shown in Figure 2 (where total force—or base shear—is plotted against pier top displacement), the measured quasi-static cyclic response was adequately reproduced numerically. Results from pushover analysis (red-colored curve) also reasonably approximate the test.

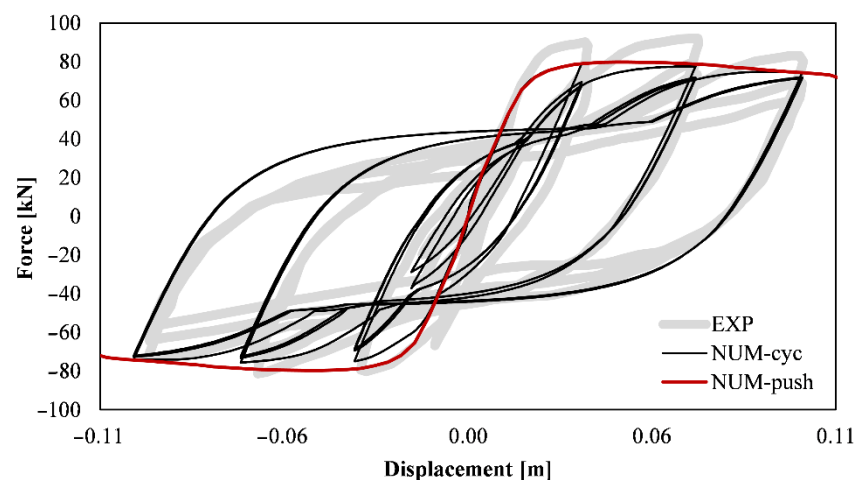


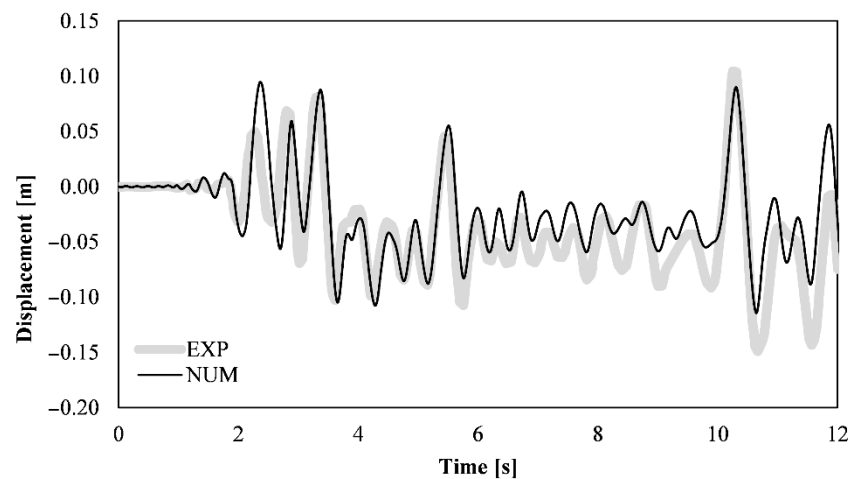
Figure 2. Experimental vs. numerical force-displacement hysteresis and predicted pushover curve.

To enable a more objective comparison, the ratio r_k , r_{BS} , r_E between test and predicted results in terms of initial stiffness (calculated at 10% of base shear), peak base shear and total energy dissipation were calculated and reported in Table 2, with uppercase signs and + indicating positive and negative loading direction, while P stands for values referred to pushover analysis. Computed indexes substantially confirmed what was discussed above, with values satisfactorily close to unity, albeit peak base shear in the positive direction was marginally overestimated.

Table 2. Ratio between experimental and numerical results in terms of initial stiffness, peak base shear and total energy dissipation.

r_k^+	r_k^-	r_{BS}^+	r_{BS}^-	r_E	r_k^+P	r_k^-P	r_{BS}^+P	r_{BS}^-P
-	-	-	-	-	-	-	-	-
0.91	1.10	0.85	0.95	1.07	1.11	1.23	0.84	0.98

Good agreement was also found when replicating the experimentally-observed dynamic shake table response of the tester pier, as it can be gathered from Figure 3, which shows the results obtained using 5% tangent–stiffness proportional damping. Compared displacement time histories are indeed in phase and, despite minor dissimilarities, peak values have been captured with sufficient accuracy. Ratios r_d between experimental and numerical maximum displacement are 0.89 (r_d^+) and 0.99 (r_d^-), significantly improved with respect to the original results of Petrini et al. [26], i.e., 0.70 and 0.89 along positive and negative direction, respectively. Given the encouraging results obtained, the same FB-FEM models were used for conducting the analyses described in the next section.

**Figure 3.** Experimental vs. numerical pier top displacement time-history.

4. Numerical Idealization of Corrosion-Induced Damage

In numerical modeling applied to earthquake engineering problems, the effects of corrosion phenomena are often conveniently represented through a change in geometry and/or material properties of concrete, rebars, and bond. Therefore, as discussed in [7], three main approaches and/or their combinations are typically adopted depending on corrosion-induced damage type, extent and location:

1. Concrete: (a) removal of spalled concrete by reducing concrete geometry; (b) reduction of cracked concrete properties around corroded reinforcement or of entire section.
2. Steel rebars: (a) decrease reinforcement area; (b) reduction of reinforcement ductility $\mu = \epsilon_s' / \epsilon_s$ (i.e., ratio between ultimate strain of corroded reinforcement vs. that of the intact one) and/or yield strength.
3. Bond: reduction of bond strength.

Measured mass loss of reinforcements due to corrosion (expressed in percentage form and calculated as $1 - (\phi' / \phi)^2$, where ϕ' is corroded rebar diameter, see [24]) is typically used to empirically infer the abovementioned artificial changes in geometry/properties, as depicted in Figure 4, where the experimentally-based simplified relationships derived by Shetty et al. [17] (Equation (1)), Coronelli and Gambarova [31] (Equation (2)), Du et al. [20] (Equation (3)), and Cairns et al. [32] (Equation (4)), extensively used in FB-FEM applications (e.g., [10,23]) are plotted using the values in Table 1. Bond degradation and local reduction of cracked concrete properties are instead seldom employed, given the intrinsic limitations

of fiber-based idealization where rebars are not explicitly modeled. Nonetheless, recent upgrades to this initial scheme allowed to overcome the issue above to be overcome and by introducing a zero-length section added at the base of the RC members, which accounts for accounted for bond-slip introducing a zero-length section at the base of the RC members, which considers the horizontal deformations components [23,24]. Another ideally suitable, yet not fully investigated using FB-FEM models, method is the Embedded Element Method, an experimentally validated analytical procedure that involves the addition of an equivalent bond strain to that of the rebar, thus decreasing its effective stiffness. It is noted that since bond failure was not a predominant phenomenon during the experiment [26], the latter has been neglected in this work. As further discussed below, this simplified approach might not be appropriate for all applications, and could lead to incorrect results.

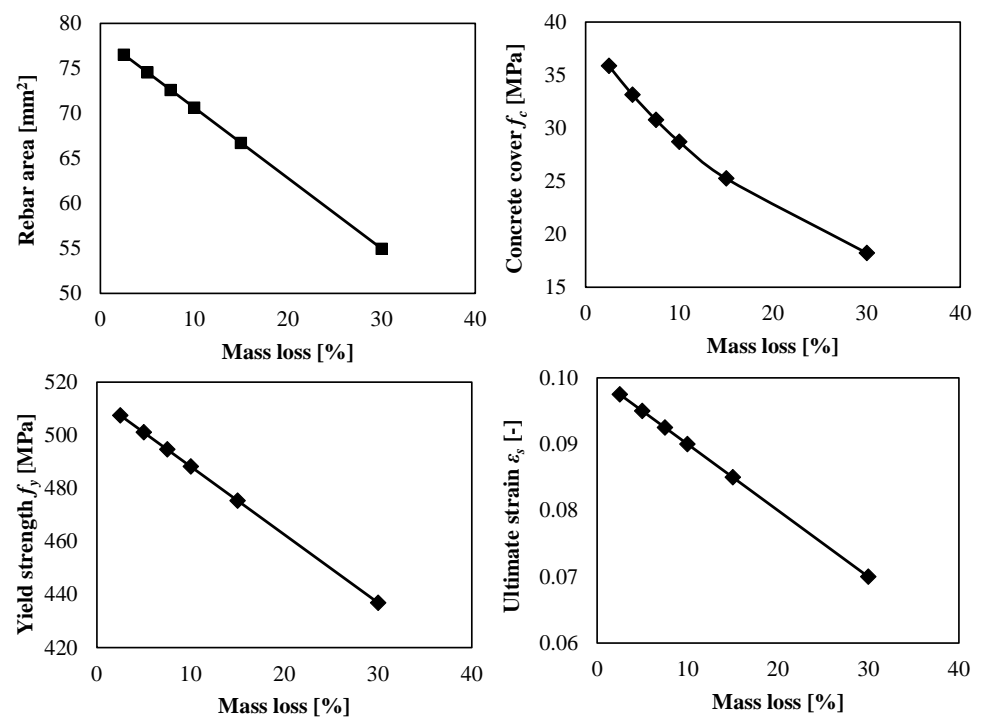


Figure 4. Typical rebar mass loss vs. property degradation empirical relationships.

In Equations (1)–(4) below, the prime symbol, $'$, indicates material properties altered (i.e., reduced) by corrosion; W_{loss} stands for percentage weight loss of rebar after corrosion; Q_{corr} is the amount of corrosion of reinforcement calculated using Equation (5) (with W weight of intact rebar and W_n weight of the same reinforcement after it was corroded and cleaned in acid solution); A_{corr} is the average cross-sectional loss expressed as a percentage of the original value and α is an empirical coefficient depending on different exposure environments. The reported α coefficient varies from 0 to 0.06 and is assumed equal to 0.01 in this endeavor as suggested in [32], which corresponds to a situation when the reduction in ductility is proportional to the average cross-sectional loss.

$$\phi' = \phi \sqrt{(1 - w_{loss}/100)} \quad (1)$$

$$f'_c = f_c \left(1 + 0.1 \frac{\epsilon'_c}{\epsilon_c}\right)^{-1} \quad (2)$$

$$f'_y = f_y (1 - 0.005 Q_{corr}) \quad (3)$$

$$\epsilon'_s = \epsilon_s (1 - \alpha A_{corr}) \quad (4)$$

Expressions employed for computing Equations (2) and (3) are reported below, where P (Equation (6)) stands for the perimeter of the intact column section, n_{bars} (Equation (7)) is the number of bars in column section, and w_{cr} (Equation (7)) is the total crack width for a given corrosion level P_{ave} (interpreted as the average corrosion penetration depth based on the uniform volumetric mass loss). In addition, v_{rust} (Equation (8)) is the ratio of the volumetric expansion of the corrosion products with respect to the uncorroded steel (suggested value is $v_{rust} = 2$, see [24]).

$$Q_{corr} = 0.01(W - W' + W_n - W'_n)/W \quad (5)$$

$$\varepsilon'_c = f_c(P' - P)^{-1} \quad (6)$$

$$P' - P = n_{bars}w_{cr} \quad (7)$$

$$w_{cr} = 2\pi(v_{rust} - 1)P_{ave} \quad (8)$$

Despite being widely employed by practitioners and applied researchers to take into account impact of corrosion attack, the implications on FB-FEM-predicted seismic responses of selecting one—or more—of the relationships reported above and depicted in Figure 4 have not been fully investigated yet, and virtually never applied, as far as the authors are aware of, to hollow-section circular RC piers. In what follows, given the lack of experimental data on the latter structural typology, additional simplified assumptions had to be introduced, i.e., uniform corrosion along the pier only impacting longitudinal reinforcements. These initial hypotheses, albeit plausible, inevitably represent only a small fraction of all the possible scenarios, thus warranting further investigations.

5. Impact of Different Corrosion Modeling Strategies on Predicted Seismic Response

To study the seismic response of RC circular hollow-section bridge piers under various levels of corrosion-induced damage and scrutinize how FB-FEM results are affected by individual and combined use of the formulae above, the numerical models validated against experimental tests in the previous section are herein employed and subjected to four main types of analyses and loads: (i) quasi-static cyclic and (ii) dynamic shake-table loading protocol used experimentally; (iii) pushover, (iv) IDA [33], where the original test PGA was replaced by PGA' , progressively increased from $PGA'/PGA=0.05$ to 1.50, enabling the investigation of the response from minor damage to collapse.

In Figure 5, the quasi-static hysteretic responses predicted by the calibrated FB-FEM models are shown. The focus of this preliminary analysis is the difference between numerical results obtained reducing diameter alone (i.e., NUM-X, where X is % of steel mass loss), reducing diameter and yield strength (i.e., NUM-X- f_y), and reducing diameter and accounting for cover loss. Before commenting on the predicted outcomes, it should be noted that only results associated with 15% and 30% mass loss were plotted, since minor differences below 15% were observed. As per the cover loss, the implementation of Equation (2) into the concrete cover region (see Figure 1a) of the associated FB-FEM model was found impractical, highly time-consuming in terms of geometric modeling, and resulting in numerical convergence issues. Thus, before undertaking such a tedious modeling exercise, the concrete cover was removed altogether (i.e., assuming the worst-case, yet not plausible scenario where corrosion induced spalling of the entire concrete cover) and coupled with a 15% mass loss to investigate upper-bound impact on results. As it can be observed, only slight differences between NUM-15 and NUM-15c (i.e., where the whole concrete section featured reduced compressive strength) are observable, corresponding to a 12% and 4% reduction of positive and negative peak base shear respectively; even lesser values were computed when comparing dissipated energy. Therefore, it was concluded that the detailed modeling of cover loss deterioration can be neglected when dealing with the specific type of RC hollow sections of bridge piers considered herein since expected differences would have been even smaller; this factor was indeed excluded in pushover and IDA analyses.

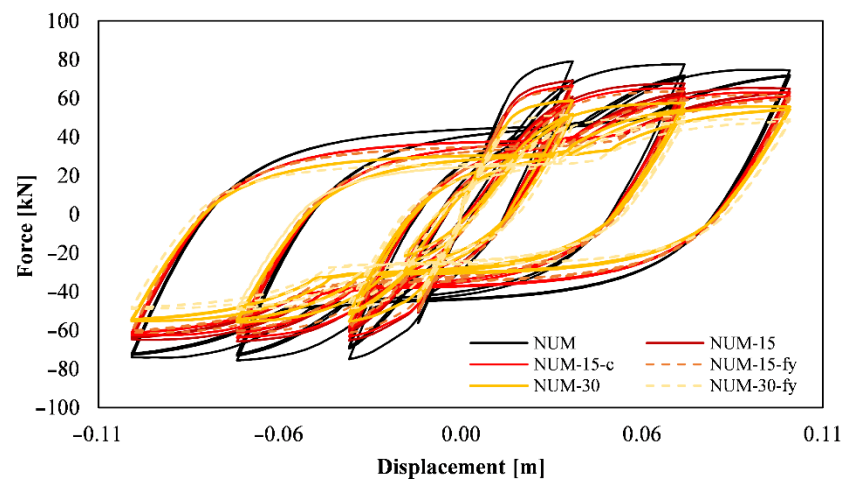


Figure 5. Impact of corrosion modeling on predicted quasi-static cyclic response: numerical force-displacement hysteresis curves accounting for rebar area reduction and reduced yield strength.

Comparisons between results obtained using models with intact properties and reducing rebar diameters indicate significant reductions in terms of both base shear, ranging from 14% (NUM-15) to 27% (NUM-30), and dissipated energy, from 18% to 34%. The influence of reducing the yield strength of longitudinal reinforcement is noticeable, and increased gap with intact behavior up to 19% (NUM-15- f_y) and 37% (NUM-30- f_y) for base shear, and 21% and 43% for dissipated energy, respectively. The observed dissimilarities are more evident when monitoring displacements, as shown in Figure 6.

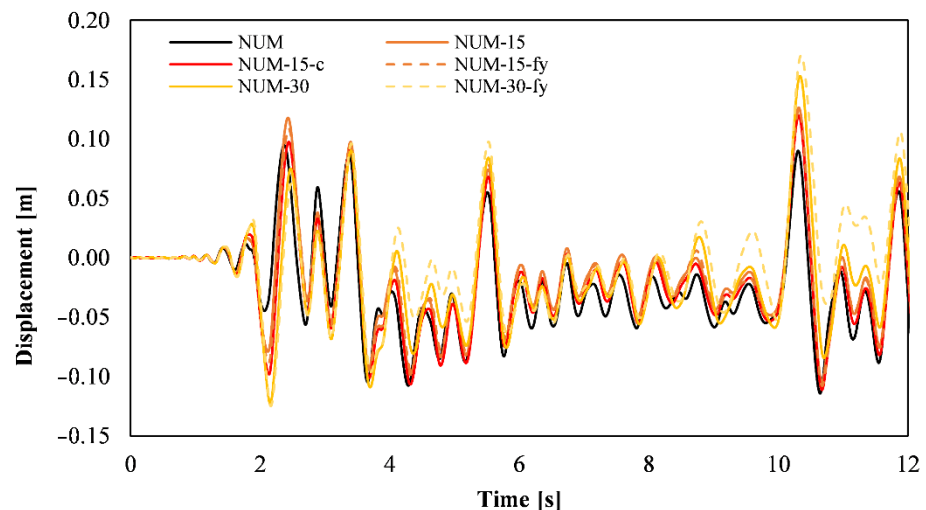


Figure 6. Impact of corrosion modeling on predicted shake-table dynamic response: numerical force-displacement hysteresis curves accounting for rebar area reduction, cover loss and reduced yield strength.

Reproducing the shake-table dynamic loading protocol further highlighted the differences between intact and corroded piers, which experienced an average increase of 35%, considering peak values. In Figure 7, the investigation is extended to ductility as well, where pushover curves are plotted against IDA points. The latter are in acceptable agreement with each other (except for the peak base shear predicted for the intact specimen, overestimated by approximately 20%), suggesting that the use of pushover analysis—notwithstanding its intrinsic limitations—is adequate when assessing the behavior of corroded RC hollow-sections under the conditions considered. Interestingly, these additional comparisons (which confirmed base shear values inferred with cyclic loading)

also enable the appreciation of the impact of such reductions on ultimate displacement capacities: differences can be observed in this sense among NUM-15 and NUM-15- $f_y-\mu$, with the former collapsing at a displacement circa 30% lower. Similar values were obtained for NUM-30 and NUM-30- $f_y-\mu$, thus indicating that the influence of ductility seems to not be proportional to the mass loss intervals selected.

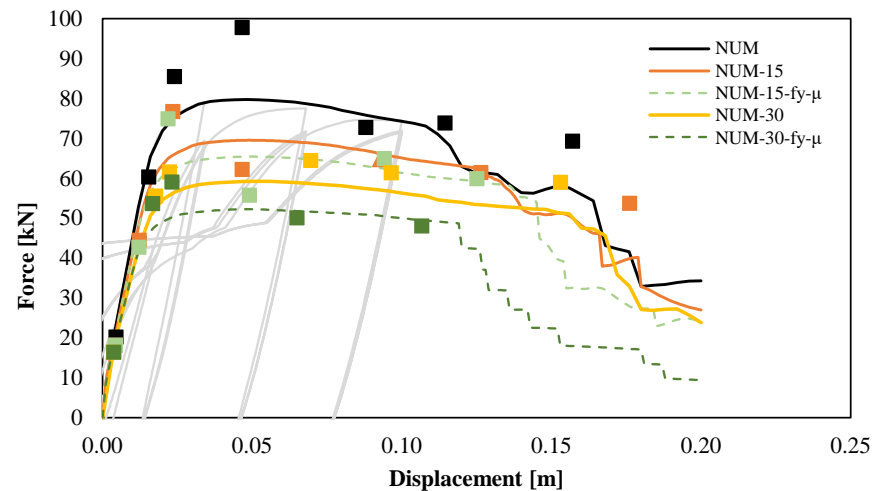


Figure 7. Impact of corrosion modeling on predicted quasi-static monotonic and shake-table dynamic response: numerical force-displacement pushover curves and IDA points accounting for rebar area reduction, reduced ductility and yield strength.

The aspects discussed above are more clearly depicted in Figure 8, where top displacement inferred via IDA are plotted against PGA'/PGA ratios. As it can be gathered, corroded piers tended to sustain lower PGA levels, whose predicted magnitude varies up to 25% depending on the modeling strategies considered, with diameter reduction models being less conservative.

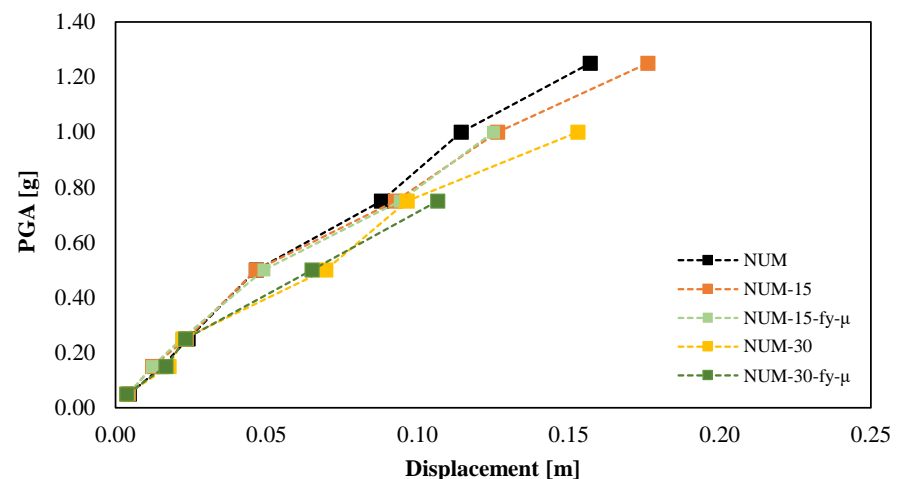


Figure 8. Impact of corrosion modeling on predicted shake-table dynamic response: IDA curves accounting for rebar area reduction, reduced ductility, and yield strength.

It is worth mentioning that despite the value of these results, considering the experimental difficulties in carrying out durability tests on corrosive aspects, the absence of dedicated guidelines, and the lack of previous laboratory evidence on the seismic response of RC hollow-section piers, the FB-FEM models presented herein and the employed empirical equations for corrosion simulation might not be readily applicable in other cases.

In particular, as already mentioned above, the influence of bond slip on the mechanical behavior should generally be considered, given its proven impact on results [34]. Further developments on this front are thus warranted.

6. Conclusions

Limited experimental work exists on the structural behavior of corroded RC hollow-sections circular bridge piers, despite being particularly vulnerable to such environmental attacks. To assess the latter aspects numerically, however, the influence of typically-employed modeling strategies on predicted responses still need to be investigated in some depth. Indeed, in current research, multiple expressions accounting for different deterioration phenomena (e.g., reduction of diameter, yield strength and ductility of steel rebars, absence of concrete cover) are often used individually or combined without considering potential implications on predicted outcomes.

In this work, the seismic response of RC hollow-sections, in both intact and corroded configurations, is investigated numerically. Influence of typically-employed simplified modeling strategies to account for corrosion-induced damage is also studied, to inform engineering professionals and applied researchers involved in assessment, rehabilitation, and retrofit processes. To this end, fiber-based finite element models (FB-FEM), widely employed by practitioners because of the reduced computational time required for performing nonlinear analyses, are developed and preliminarily validated against previous experimental tests on a reduced scale column. Both quasi-static cyclic and shake-table dynamic loading were considered experimentally, and subsequently created numerically. Good agreement was found among measured and predicted results, with only minor differences in terms of positive base shear in the cyclic analysis. Given the satisfactory results produced, the same FB-FEM models were also used for investigating parametrically corrosion impact and influence of the various modeling approaches selected.

Four main corrosion modeling strategies were considered, which account for diameter reduction of rebar alone (NUM-X models, with X steel mass loss %—two main values were studied, i.e., 15% and 30%, typically associated with moderate and severe corrosion-induced damage), diameter and yield strength reduction (NUM-X- f_y), diameter reduction and cracked concrete cover (NUM-X-c), diameter, yield strength and ductility reduction (NUM-X- f_y - μ). Devised models were subjected to cyclic and shake-table experimental protocols, as well as to pushover and incremental dynamic analyses (IDA). Interpretation of obtained results provided the practical insights summarized in the following:

- Corrosion is expected to have a significant impact on the response of RC hollow-section circular bridge piers, prompting a reduction in terms of base shear peak and ultimate displacement capacity up to 37% and 50%, respectively, depending on the simplified approach used for representing corrosion damage. Further investigations on this topic are thus warranted.
- In general, extent of predicted impact of corrosion-induced damage is proportional to modeling complexity. Therefore, when considering more simplified assumptions, non-conservative predictions can be obtained, suggesting that all the deterioration components (except that of concrete cover, see below) should be considered simultaneously in the assessment of bridges.
- Detailed modeling of concrete cover corrosion-induced damage is challenging and highly time-consuming using FB-FEM models, and may produce spurious numerical instability issues.
- To overcome this limitation and investigate the upper-bound impact of such deterioration phenomena, the concrete cover was removed altogether. Even in this case, only minor reductions in terms of positive and negative base shear (12% and 4%) and dissipated energy (9% and 3%) were observed. It is therefore concluded that the FB-FEM modeling of concrete cover damage or loss might be neglected in the specific conditions considered in this work.

- Reducing diameter alone and combining it with decreased yield strength produce markedly different results in cyclic analyses, with dissimilarities slightly increasing when considering larger corrosion rates. NUM-X- f_y models generally provided values 5–10% lower with respect to NUM-X, in terms of both peak base shear and dissipated energy. Dynamic analyses indicated approximately 15–20% differences in terms of peak top displacements.
- When also adding ductility reductions, FB-FEM results tended to exhibit lower collapse displacement capacities, with an average 30% difference between NUM-X and NUM-X- f_y - μ results, which seem to not increase with increased corrosion rates. Further, NUM-X- f_y - μ models tended to sustain PGAs 25% larger than their NUM-X counterparts.

Author Contributions: Conceptualization, N.S. and D.M.; methodology, N.S. and D.M.; formal analysis, N.S. and T.Q.; investigation, N.S. and D.M.; resources, N.S. and D.M.; data curation, N.S. and D.M.; writing—original draft preparation, D.M.; writing—review and editing, N.S. and D.M.; supervision, D.M.; project administration, D.M. All authors have read and agreed to the published version of the manuscript.

Funding: This research received no external funding.

Institutional Review Board Statement: Not applicable.

Informed Consent Statement: Not applicable.

Data Availability Statement: Data available upon request.

Acknowledgments: The quality of the manuscript benefited from the insightful comments of two anonymous reviewers, whose contribution is gratefully acknowledged.

Conflicts of Interest: The authors declare no conflict of interest.

References

1. Calvi, G.M.; Moratti, M.; O'Reilly, G.J.; Scattarreggia, N.; Monteiro, R.; Malomo, D.; Calvi, P.M.; Pinho, R. Once upon a Time in Italy: The Tale of the Morandi Bridge. *Struct. Eng. Int.* **2019**, *29*, 198–217. [[CrossRef](#)]
2. Koch, G.H.; Brongers, M.P.H.; Thompson, N.G.; Virmani, Y.P.; Payer, J.H. *Corrosion Cost and Preventive Strategies in the United States*; NACE International: Houston, TX, USA, 2002.
3. Olmstead, S. Climate change adaptation and water resource management: A review of the literature. *Energy Econ.* **2014**, *46*, 500–509. [[CrossRef](#)]
4. Angst, U.M. Challenges and opportunities in corrosion of steel in concrete. *Mater. Struct. Constr.* **2018**, *51*, 4. [[CrossRef](#)]
5. Tan, J.-S.; Elbaz, K.; Wang, Z.-F.; Shen, J.S.; Chen, J. Lessons Learnt from Bridge Collapse: A View of Sustainable Management. *Sustainability* **2020**, *12*, 1205. [[CrossRef](#)]
6. Diaz, E.E.M.; Moreno, F.N.; Mohammadi, J. Investigation of Common Causes of Bridge Collapse in Colombia. *Pract. Period. Struct. Des. Constr.* **2009**, *14*, 194–200. [[CrossRef](#)]
7. Hanjari, K.Z.; Kettil, P.; Lundgren, K. Analysis of Mechanical Behavior of Corroded Reinforced Concrete Structures. *ACI Struct. J.* **2011**, *108*, 532–541. [[CrossRef](#)]
8. Aquino, W.; Hawkins, N.M. Seismic Retrofitting of Corroded Reinforced Concrete Columns Using Carbon Composites. *ACI Struct. J.* **2007**, *104*, 348–356. [[CrossRef](#)]
9. Ma, Y.; Che, Y.; Gong, J. Behavior of corrosion damaged circular reinforced concrete columns under cyclic loading. *Constr. Build. Mater.* **2012**, *29*, 548–556. [[CrossRef](#)]
10. Cheng, H.; Li, H.-N.; Wang, D.-S. Prediction for lateral deformation capacity of corroded reinforced concrete columns. *Struct. Des. Tall Spec. Build.* **2019**, *28*, e1560. [[CrossRef](#)]
11. Zhang, J.; Peng, H.; Cai, C.S. Destructive Testing of a Decommissioned Reinforced Concrete Bridge. *J. Bridg. Eng.* **2013**, *18*, 564–569. [[CrossRef](#)]
12. Aghl, P.P.; Naito, C.J.; Riggs, H.R. Full-Scale Experimental Study of Impact Demands Resulting from High Mass, Low Velocity Debris. *J. Struct. Eng.* **2014**, *140*, 04014006. [[CrossRef](#)]
13. Tapan, M.; Aboutaha, R. Effect of steel corrosion and loss of concrete cover on strength of deteriorated RC columns. *Constr. Build. Mater.* **2011**, *25*, 2596–2603. [[CrossRef](#)]
14. Malomo, D.; Scattarreggia, N.; Orgnoni, A.; Pinho, R.; Moratti, M.; Calvi, G.M. Numerical Study on the Collapse of the Morandi Bridge. *J. Perform. Constr. Facil.* **2020**, *34*, 04020044. [[CrossRef](#)]
15. Yuan, Z.; Fang, C.; Parsaeimaram, M.; Yang, S. Cyclic Behavior of Corroded Reinforced Concrete Bridge Piers. *J. Bridg. Eng.* **2017**, *22*, 04017020. [[CrossRef](#)]

16. Domaneschi, M.; De Gaetano, A.; Casas, J.R.; Cimellaro, G.P. Deteriorated seismic capacity assessment of reinforced concrete bridge piers in corrosive environment. *Struct. Concr.* **2020**, *21*, 1823–1838. [[CrossRef](#)]
17. Shetty, A.; Venkataramana, K.; Narayan, K.S.B. Experimental and numerical investigation on flexural bond strength behavior of corroded NBS RC beam. *Int. J. Adv. Struct. Eng.* **2015**, *7*, 223–231. [[CrossRef](#)]
18. The Modified Compression-Field Theory for Reinforced Concrete Elements Subjected to Shear. *ACI J. Proc.* **1986**, *83*, 219–231. [[CrossRef](#)]
19. Di Carlo, F.; Meda, A.; Rinaldi, Z. Numerical evaluation of the corrosion influence on the cyclic behaviour of RC columns. *Eng. Struct.* **2017**, *153*, 264–278. [[CrossRef](#)]
20. Du, Y.G.; Clark, L.A.; Chan, A. Residual capacity of corroded reinforcing bars. *Mag. Concr. Res.* **2005**, *57*, 135–147. [[CrossRef](#)]
21. Di Sarno, L.; Pugliese, F. Numerical evaluation of the seismic performance of existing reinforced concrete buildings with corroded smooth rebars. *Bull. Earthq. Eng.* **2020**, *18*, 4227–4273. [[CrossRef](#)]
22. Chiara, C.; Rui, P. Seismic response of continuous span bridges through fiber-based finite element analysis. *Earthq. Eng. Eng. Vib.* **2006**, *5*, 119–131. [[CrossRef](#)]
23. Rao, A.S.; Lepech, M.D.; Kiremidjian, A.S.; Sun, X.-Y. Simplified structural deterioration model for reinforced concrete bridge piers under cyclic loading. *Struct. Infrastruct. Eng.* **2017**, *13*, 55–66. [[CrossRef](#)]
24. Dizaj, E.A.; Madandoust, R.; Kashani, M.M. Exploring the impact of chloride-induced corrosion on seismic damage limit states and residual capacity of reinforced concrete structures. *Struct. Infrastruct. Eng.* **2018**, *14*, 714–729. [[CrossRef](#)]
25. Chen, J.; Wang, J.; Zhu, J.-H.; Feng, Y.; Liu, C.-B. Study on the Corroded Hollow Section RC Columns Strengthened by ICCP-SS System. *Buildings* **2021**, *11*, 197. [[CrossRef](#)]
26. Petrini, L.; Maggi, C.; Priestley, M.J.N.; Calvi, G.M. Experimental Verification of Viscous Damping Modeling for Inelastic Time History Analyses. *J. Earthq. Eng.* **2008**, *12*, 125–145. [[CrossRef](#)]
27. Seismosoft. SeismoStruct—A Computer Program for Static and Dynamic Nonlinear Analysis of Framed Structures. 2019. Available online: <https://seismosoft.com> (accessed on 23 July 2021).
28. Menegotto, M.; Pinto, P. Method of analysis for cyclically loaded RC plane frames including changes in geometry and non-elastic behavior of elements under combined normal force and bending. In Proceedings of the IABSE Symposium on Resistance and Ultimate Deformability of Structures Acted on by Well Defined Repeated Loads, Zurich, Switzerland, 27 August 1973; pp. 15–22.
29. Mander, J.B.; Priestley, M.J.N.; Park, R. Theoretical Stress-Strain Model for Confined Concrete. *J. Struct. Eng.* **1988**, *114*, 1804–1826. [[CrossRef](#)]
30. Martínez-Rueda, J.E.; Elnashai, A.S. Confined concrete model under cyclic load. *Mater. Struct. Constr.* **1997**, *30*, 139–147. [[CrossRef](#)]
31. Coronelli, D.; Gambarova, P. Structural Assessment of Corroded Reinforced Concrete Beams: Modeling Guidelines. *J. Struct. Eng.* **2004**, *130*, 1214–1224. [[CrossRef](#)]
32. Cairns, J.; Plizzari, G.A.; Du, Y.; Law, D.W.; Franzoni, C. Mechanical properties of corrosion-damaged reinforcement. *ACI Mater. J.* **2005**, *102*, 256–264. [[CrossRef](#)]
33. Vamvatsikos, D.; Cornell, C.A. Direct estimation of the seismic demand and capacity of oscillators with multi-linear static pushovers through IDA. *Earthq. Eng. Struct. Dyn.* **2006**, *35*, 1097–1117. [[CrossRef](#)]
34. Dehestani, M.; Mousavi, S. Modified steel bar model incorporating bond-slip effects for embedded element method. *Constr. Build. Mater.* **2015**, *81*, 284–290. [[CrossRef](#)]